Table of Contents

	Page	
List of Figures	iv	1/A2
List of Tables	v	1/A3
Glossary of Symbols	1	1/A7
I. Introduction	2	1/A14
II. Cloud Microphysics	5	1/A11
A. Implicit Model	5	1/A11
B. Explicit Model	6	1/A12
1. Diffusion Equations	6	1/A12
2. Energy Balance	7	1/A13
3. Relative Values of Energy Terms	9	1/B1
4. Solution of Explicit Model for Two Volatile Components	16	1/B8
5. Numerical Procedure	18	1/B10
6. Verification	18	1/B10
References	22	1/B14
III. Meso-Scale Model	23	1/C1
A. Introduction	23	1/C1
B. Basic Equations	23	1/C1
C. Boundary Conditions	27	1/C5
1. Lateral Boundaries	27	1/C5
2. Bottom Boundary	27	1/C5
D. Initial Conditions	27	1/C5
E. Cloud and Precipitation Parameterization	28	1/C6
1. Stable Precipitation	28	1/C6
2. Convective Precipitation	29	1/C7
F. Boundary-Layer Parameterization	31	1/C9
G. Numerical Methods	37	1/D1
1. Model Structure	37	1/D1
2. Numerical Schemes	37	1/D1
References	42	1/D6
IV. Input Data on Equilibrium Vapor Pressures for HCL and H_2O over HCl_{aq}	44	1/D8
A. Form of Curves	45	1/D9
B. Procedure	47	1/D11
References	58	1/E8

List of Figures

Figure No.		Page	
2.1	Droplets per cm^3 per Micron Radius Interval- 100 meters above cloud base, steady updraft.	19	1/B11
2.2	Droplets per cm^3 per Micron Radius Interval- 100 meters above cloud base, turbulent motion.	21	1/B13
3.1	The horizontal grid-net superimposed on the region of simulation in the meso-scale model.	38	1/D2
4.1	Coefficients A_0 vs μ and the Smoothed Curve $A_3(\mu)$.	51	1/E1
4.2	Coefficients B_0 vs μ and the Smoothed Curve $B_2(\mu)$.	52	1/E2
4.3	Coefficients C_0 vs μ and the Smoothed Curve $C_1(\mu)$.	53	1/E3
4.4	Coefficients A' vs μ and the Smoothed Curve $A_1'(\mu)$.	55	1/E5
4.5	Coefficients B' vs μ and the Smoothed Curve $B_2'(\mu)$.	56	1/E6
4.6	Coefficients C' vs μ and the Smoothed Curve $C_3'(\mu)$.	57	1/E7

List of Tables

Table No.		Page	
1.1	Scales of Meteorological Systems and Processes	4	1/A10
2.2	Relative Values of the Energy Terms for $\{(NH_4)_2SO_4\}$.	11	1/B3
2.3	Estimates of the Energy Terms in Relation to Q_T for the HCl/H_2O System (see Text) at $\mu = 4$.	14	1/B6
3.1	Height of Fixed Vertical Level	39	1/D3
4.1	Numerical values of the Coefficients A_0, B_0, C_0 for Molalities $0 \leq \mu \leq 15.88$.	49	1/D13

FEB 1 0 1978

NAS 1.26 :2928

NASA Contractor Report 2928

COMPLETED
ORIGINAL

Rain Scavenging of Solid Rocket Exhaust Clouds

A. Nelson Dingle

GRANT NSG-1243
JANUARY 1978

NASA

105

NAS1.26:2928

NASA Contractor Report 2928

Rain Scavenging of Solid Rocket Exhaust Clouds

A. Nelson Dingle
University of Michigan
Ann Arbor, Michigan

Prepared for
Langley Research Center
under Grant NSG-1243

National Aeronautics
and Space Administration

Scientific and Technical
Information Office

1978

BLANK PAGE

Glossary of Symbols

c	specific heat
D	diffusion coefficient, $cm^2 sec^{-1}$
e	vapor pressure, dynes cm^{-2}
E	equivalent grey body emissivity
F	correction factor (Fuchs, 1959)
h	enthalpy of solution per unit mass
K	thermal conductivity of air
m	mass, gm
M	molecular weight, gm per mole
n	number density of particles or droplets, cm^{-3}
r	radius of droplet, cm
R	specific gas constant, ergs $gm^{-1} \cdot K^{-1}$
t	time, sec
T	temperature, °K
V	ventilation coefficient (Squires, 1952)
x	mixing ratio, gm per gm of dry air
μ	molality of HCl_{aq}
μ_f	molecular viscosity of air
ρ	density, gm cm^{-3}
σ	surface energy, ergs cm^{-2}
σ_R	Stefan-Boltzmann constant, ergs $cm^{-2} sec^{-1} \cdot K^{-4}$

Subscripts

a	ambient air	s	saturation
i	size category	v	vapor
k	heat	w	water
r	droplet or droplet surface		

I. Introduction

In approaching the problem of the drift, dilution, removal and deposition of the SRM exhaust products, we face complexities that are in major part attributable to the very great range of the scales of atmospheric processes (Table 1.1) In modeling by numerical techniques this consideration is crucial, because a given numerical model can span only a limited domain to which the scale (and hence the associated "time constants" or "decay periods") must be restricted.

Specifically, the exhaust plume problem starts with processes of molecular scale (10^{-3}cm) as particles form in the hot concentrated exhaust gases, and we are plunged immediately into problems of coagulation, diffusion and sedimentation of particles (10^{-5}cm to 10^{+1}cm) and gases, including air and water vapor entrainment, in forming what we call the SGC. The meteorological problem, by mutual understanding, begins with the SGC, some 90 seconds after ignition: a ball of ∿250 m radius at about 500-700 m altitude, full of earth surface debris in addition to the HCl, Al_2O_3, and H_2O specifically produced by the rocket motor combustion.

We are concerned about the disposal of this SGC, and we recognize at least 3 specific kinds of processes: (1) sedimentation and dry deposition, i.e., the fallout of large ($r > 10^{-3}$cm) particles, plus the turbulent and diffusive impaction of smaller particles ($r > 10^{-4}$cm) on surface obstructions, and the direct sorption of gases ($r \sim 10^{-3}$cm)

by plants, etc; (2) scavenging by rainfall, which we shall expand upon later; and (3) diffusion, dilution and transport by atmospheric motions until background concentration levels have been reestablished.

In particular, the present effort is especially focussed upon those removal processes that involve cloud formation and rainfall. We have launched two parallel efforts in attacking this problem, one at the small scale end of the spectrum, which is called "cloud microphysics", and the other at the mesoscale (Table 1.1), which in effect sets the stage within the atmospheric environment for the development of cloud and precipitation.

Table 1.1 : Scales of Meteorological Systems and Processes.

Synoptic Systems	$\sim 10^8$ cm = 10^3 km
Mesoscale Systems	$\sim 10^7$ cm = 10^2 km
Convective Showers	$\sim 10^6$ cm = 10 km
Individual Clouds	$\sim 10^5$ cm = 1 km
Air Turbulence	10^4 - 10^0 cm
Rain Drops	10^{-2} - 10^{-1} cm
Cloud Droplets	10^{-3} - 10^{-2} cm
Nuclei	10^{-6} - 10^{-3} cm
Mean Free Path	$\sim 10^{-5}$ cm
H_2O Molecule	3×10^{-8} cm

II. Cloud Microphysics

Cloud microphysics encompasses the processes of cloud droplet nucleation, growth and coalescence, which serve to incorporate the constituents of the local atmosphere into the cloud elements, and to convert cloud to precipitation.

A. The Implicit Model

The diffusive growth of a droplet of pure substance from its vapor phase may be expressed by the modified Maxwell diffusion equation:

$$\frac{dm}{dt} = \frac{4\pi r D F_v V}{R} \left(\frac{e_a}{T_a} - \frac{e_r}{T_r}\right) \qquad (1)$$

In this expression

F_v is the correction factor due to Fuchs (1959) which resolves the continuum vapor flux with that given by kinetic theory at and near the surface of small droplets; and

V is the ventilation coefficient of Squires (1952) adapted from Frossling (1938).

All other symbols follow their customary meteorological usage, and are defined in the glossary, p. 4.

To complete the basic model of droplet growth, the heat transfer from the growing droplet must be considered and balanced against the latent energy released:

$$L \frac{dm}{dt} = 4\pi r K F_K V (T_r - T_a) \qquad (2)$$

Mason (1957) devised a procedure involving a series of approximations and assumptions, whereby (1) and (2) are combined into a single growth equation that depends only upon the saturation ratio, $S = e/e_s(T_a)$, and the air temperature, T_a:

$$r \frac{dr}{dt} = \frac{S-1}{a+b} \tag{3}$$

where $a = L^2\rho_L/(KRT_a^2)$; $b = \rho_L RT_a/e_s(T_a)D$.

The growth equation, (3) has been widely used for the computation of cloud droplet growth upon particles composed wholly or partially of soluble inorganic salts. Because the droplet temperature, T_r, is not explicitly required to solve (3), this system is referred to as the implicit model.

B. The Explicit Model

In its simplest conception, the HCl-H_2O system with which we must deal in the case of the solid rocket motor (SRM) exhaust products, involves two volatile components and their interactions. Clearly, therefore, the microphysical problem must be reexamined.

1. The Diffusion Equations

When HCl and H_2O vapors are present together, they jointly determine the equilibrium vapor pressure of each component over an HCl_{aq} droplet, and Mason's principal simplifying steps are inapplicable. It is assumed that the two vapors may be treated as if they diffuse independently, so that the change of mass of a solution droplet may be

expressed as

$$dm_r = dm_1 + dm_2 \tag{4}$$

where the subscripts indicate the respective components, i.e., H_2O and HCl. Then, analogously with equation (1)

$$\frac{dm_1}{dt} = \frac{4\pi r D_1 F_{v_1} V}{R_1} \left(\frac{e_{a_1}}{T_a} - \frac{e_{r_1}}{T_r}\right) \tag{5}$$

and

$$\frac{dm_2}{dt} = \frac{4\pi r D_2 F_{v_2} V}{R_2} \left(\frac{e_{a_2}}{T_a} - \frac{e_{r_2}}{T_r}\right) \tag{6}$$

2. The Energy Balance

The energy balance of the droplet may be expressed by

$$Q_T = Q_L + Q_K + Q_R - Q_\sigma + Q_M + Q_F + Q_D \tag{7}$$

where the Q's are defined as follows:

$Q_T = m_r c_r \frac{dT_r}{dt}$ internal energy increase (7a)

$Q_L = Q_{L_1} + Q_{L_2}$ latent energy release (7b)

$Q_{L_1} = L_1 \, dm_1/dt; \quad Q_{L_2} = L_2 \, dm_2/dt$

$Q_K = -4\pi r K F_K V (T_r - T_a)$ conductive heat transfer from drop (7c)

$Q_R = -16\pi r^2 \sigma_R E T_a^3 (T_r - T_a)$ radiative transfer from drop (7d)

$$Q_r = 4\pi r^2 \left[\frac{2\sigma}{3}\left(\frac{1}{m_r}\frac{dm_r}{dt} + \frac{\mu}{\rho_r}\frac{\partial \rho_r}{\partial \mu}\left(\frac{1}{m_1}\frac{dm_1}{dt} - \frac{1}{m_2}\frac{dm_2}{dt}\right)\right)\right.$$
$$\left. - \mu \frac{\partial r}{\partial \mu}\left(\frac{1}{m_1}\frac{dm_1}{dt} - \frac{1}{m_2}\frac{dm_2}{dt}\right) + \frac{dT_r}{dt}\left(\frac{\partial \sigma}{\partial T} - \frac{2\sigma}{3}\frac{1}{\rho_r}\frac{\partial \rho_r}{T}\right)\right]$$

surface increase energy (7e)

$$Q_M = - c_r(T_r - T_a)\frac{dm_r}{dt} \qquad \text{mixing} \quad (7f)$$

$$Q_F = \frac{2r^2 m_r g^2}{9\mu_f}(\rho_r - \rho_a) \qquad \text{frictional conversion} \quad (7g)$$

$$Q_D = \frac{\mu}{m_r}\frac{dh}{d\mu}\frac{dm_r}{dt} \qquad \text{heat of dilution} \quad (7h)$$

The latent energy term (7b) accounts for phase changes of both H_2O and HCl in the present context. Although L_2 is about 17 kcal mol^{-1} as against an L_1 value of about 10.7 kcal mol^{-1}, at most stages of growth $\frac{dm_1}{dt} > \frac{dm_2}{dt}$, and the heat requirement/contribution of HCl phase changes may be comparable to that for H_2O. The radiative transfer term (7d) depends upon the value of the equivalent grey body emissivity, E, which is not precisely known. We estimate that it lies within the range of 0.7 to 0.9 or so for the infrared region of concern. The surface energy term (7e), because of dependency of both solution density and surface tension upon molality and temperature, is quite complicated. The mixing term (7f) accounts for condensation of vapors at air temperature, T_a, and subsequent adjustment of the liquid increment to the droplet temperature, T_r. For an evaporating droplet, Q_M is assumed to be zero. The friction term (7g) accounts for the conversion of potential energy to heat by dissipation at terminal fall speed. It is obviously very small (see below) for cloud droplets. The dilution term (7h) accounts for the requirement/contribution of heat as the HCl_{aq} solution changes in concentration.

Enthalpy of dilution is tabulated in standard chemical references (e.g., Weast, 1971).

3. Relative Values of the Energy Terms

The system (4), (5), (6), (7) may be regarded as being applicable to any number of volatile components, as long as one allows that additional energy terms for interactive heat sources and sinks may be added to (7) as written above. In the present work we are directly concerned with the H_2O-HCl system involving also the solid Al_2O_3 exhaust products of the SRM. We shall therefore de-emphasize the broader generalization of the present scheme and focus upon its application to the SRM exhaust problem.

To simplify (7) for the immediate purpose, it is useful to make an order of magnitude comparison among the respective energy balance terms. Obviously Q_L and Q_K are the largest terms. They have opposing effects upon the droplet temperature, T_r, and are effectively differenced in the process of computing T_r. In fact, the fundamental assumption that permits elimination of T_r from the implicit model growth equation is that Q_L and Q_K are identically equal. We note, however, that this is only approximately true, and that, indeed, the actual growth rate is necessarily dependent upon the residual between Q_L and Q_K. Terms in the energy balance equation that are of the same magnitude as this residual must therefore be considered non-negligible for the explicit model.

Utilizing output from implicit model calculations of

the growth of cloud droplets on a population of $(NH_4)_2SO_4$ nuclei in a 1 m sec^{-1} updraft 20 m above cloud base, estimates of the respective terms of (7) have been computed and are presented in Table 2 as multiples of Q_T, the internal energy (heat storage) term. It is clearly shown for this case that Q_L and Q_K are 3 to 5 orders of magnitude larger than Q_T for droplets up to 10 μm radius. This ratio diminishes as drop size increases, and will be much smaller for 100 to 1000 μm-radius raindrops. Terms within one order of magnitude of Q_T are Q_R, Q_M and Q_σ, each of which diminishes with increasing droplet size. Inasmuch as Q_T is an increasing function of droplet size, it contributes to the diminution of the above ratios as droplets become larger. The absolute values of Q_T are therefore given at the bottom of the table in units of erg sec^{-1}. The frictional term increases with droplet size inasmuch as it depends mainly upon droplet terminal fall speed. Obviously the values for cloud droplets are so small (11 to 15 orders of magnitude less than Q_T) as to be totally negligible for modelling purposes. We note however that fall speeds for these droplets are of order 10^3 less than those of raindrops, for which therefore the frictional term should be about 10^6 larger. The dilution term, Q_D, is also quite negligible for $(NH_4)_2SO_4$ in cloud droplets, but may become marginally significant for raindrops. The dilution heat for HCl is much larger. For 4.0 molal aquaeous HCl droplets, Q_D/Q_T takes values of 370, 29 and 11 respectively for droplets of radius 1, 5 and 10 μm growing at the rates derived from the above implicit model calculations. Thus, for the HCL/H_2O system, the heat of dilution is substantial.

Table 2.2 : Relative Values of the Energy Terms for $\{(NH_4)_2SO_4\}$.*

	r = 1 μm	r = 5 μm	r = 10 μm
Q_L/Q_T	5.913E4	4.461E3	1.719E3
Q_K/Q_T	5.911E4	4.456E3	1.716E3
Q_R/Q_T	16.0	4.92	3.55
Q_σ/Q_T	3.34	5.16E-2	1.02E-2
Q_M/Q_T	2.62	4.40E-1	2.53E-1
Q_F/Q_T	1.59E-15	2.58E-14	9.13E-12
Q_D/Q_T	1.07E-6	3.82E-4	5.9E-3
For 4.0 molal HCl_{aq}:			
Q_D/Q_T	370	29	11

*Nuclei vertical rise rate of 1 m sec^{-1}; 20 m above cloud base.

The contribution of Q_{L_2} deserves specific mention. The molar latent heat, L_2, released as HCl makes the vapor-liquid transition of the order of 1.7 x L_1. Because this heat warms the drop, it must operate to slow droplet growth of the relatively pure H_2O droplets in a mixed population having a uniform environment, as they acquire HCl from the vapor more rapidly than their neighbors. However, as the SGC progresses in time, the HCl partial pressure is expected to decrease rapidly in response not only to the solvation in droplets, but also because of turbulent dilution of the cloud by environmental air. It is expected that, at some point, the dilution will reverse the HCl vapor pressure gradient, whereupon HCl will begin to leave the liquid phase, and L_2 will be extracted from, rather than released to, the aquaeous HCl droplets. The cooling effect of this process must then contribute to an increased condensation of H_2O from the air, and may be an important mechanism for accelerating the onset of rain. That this capability is particularly a property of the most strongly acidic droplets is also of particular significance in determining the deposition pattern of aquaeous HCl.

An additional attempt to adapt the implicit model output to the study of the HCl/H_2O system was made. In this case the values after 10 sec of upward displacement from cloud base at 1 m sec^{-1} speed were adapted from the $(NH_4)_2SO_4$ calculations. The model values for dm/dt, m_w, and dT_r/dt for $(NH_4)_2SO_4$ nuclei, (T_r-T_a), and μ are

	r = 0.1 μm	1.0 μm	10 μm
dm/dt	9.4E-16	1.66E-12	9.8E-11
m_w	4.42E-15	3.83E-12	4.96E-9
dT_r/dt	8.6E-3	6.0E-3	6.0E-3
T_r-T_a	2.11E-4	1.46E-2	7.11E-2
μ	1.55E-1	4.4E-3	9.8E-2

at 10 m above cloud base. Using these values as if they were directly applicable to HCl/H_2O condensation, the figures in Table 3 are computed. The droplet of r=1 μm grows more rapidly relative to its mass than the 0.1 μm and 10 μm droplet. It is also the most dilute of the droplets presented (see above). The dilution term is similar in relative magnitude to its value at 20 m above cloud base (above). For other HCl concentrations, multiply Q_D/Q_T by $(\mu/4)^2$. Clearly the relative magnitudes of the respective energy terms depend upon droplet size, rate of growth and chemical species; and different stages in the processes of condensation, evaporation, coalescence and precipitation may permit neglect of or may require retention of different terms in the energy budget. Only Q_F appears to be totally negligible, and this allows simplification of (7) to

$$Q_T = Q_L + Q_K + Q_R - Q_\sigma + Q_M + Q_D \qquad (8)$$

By means of the definitive expressions (7a-h) applied to (8), the droplet temperature elevation may be written

Table 2.3: Estimates of the Energy Terms in Relation to Q_T for the HCl/H_2O System (see text) at $T_\mu = 4$.

	r = 0.1 μm	r = 1.0 μm	r = 10 μm
Q_L/Q_T ($\tilde{\approx} Q_K/Q_T$)	1.46E4	4.28E4	1.95E3
Q_R/Q_T (E=1)	0.92	9.7	3.7
Q_σ/Q_T	8.9	2.6	0.012
Q_μ/Q_T	0.006	1.05	0.24
Q_F/Q_T	8E-15	1.2E-12	1.2E-10
Q_P/Q_T	94	276	13

$$(T_r - T_a) = \left[\frac{[Q_L + Q_D - Q_T - Q_r]}{[4\pi r(KF_K V + 4r\sigma_R E T_a^3) + C_r\, dm_r/dt]}\right] \qquad (9)$$

The diffusion equations (5), (6), and the droplet temperature elevation equation (9) represent the micro-physical processes that require evaluation within each time step for each size category of the cloud droplet spectrum. The size spectrum is usually well-enough expressed by 25 to 50 size categories.

In addition, for each time step, the mass conservation accounts are kept. Assuming no dilution of the air parcel by turbulent mixing with environmental air

$$\frac{dx_1}{dt} = -\sum_i n_i \left(\frac{dm_1}{dt}\right)_i \qquad (10)$$

$$\frac{dx_2}{dt} = -\sum_i n_i \left(\frac{dm_2}{dt}\right)_i \qquad (11)$$

The enivornmental temperature and pressure changes from one time step to another are given by

$$\frac{dp}{dt} = -wp_a\left(g + \frac{dw}{dt}\right) \qquad (12)$$

and

$$\frac{dT_a}{dt} = -\frac{\left[L_1 \frac{dx_1}{dt} + L_2 \frac{dx_2}{dt} + \left(g + \frac{dw}{dt}\right)\frac{dz}{dt}(1 + x_1 + x_2)\right]}{c_p + x_1 c_{p_1} + x_2 c_{p_2} + \sum_i (m_r c_r)_i n_i} \qquad (13)$$

where the summation in the denominator represents the heat capacity of the liquid carried with the parcel. Equations (5), (6) and (9) for each droplet size category, plus equations (10), (11), (12) and (13) constitute the explicit

model for two volatile components.

4. Solution of the Explicit Model for Two Volatile Components

a. Initialization

The values of $T_a^{(0)}$, $x_1^{(0)}$, $x_2^{(0)}$, $n(r_i)^{(0)}$, and $w^{(0)}$ are specified for time $t^{(0)} = 0$ by the statement of the problem. The values of $T_{r_i}^{(0)}$ may be determined for each droplet size category, if $m_{i_1}^{(0)}$ and $m_{i_2}^{(0)}$ are known, as follows:

1. Assume an approximate value of $T_{r_i}^{(0)}$

   $\{T_{r_i}^{(0)}\} = T_a^{(0)}$

   where { } designates an estimated value.

2. Calculate the corresponding values of

   $[\frac{dm_1^{(0)}}{dt}]$ and $[\frac{dm_2^{(0)}}{dt}]$ for each size category

   using (5) and (6). Here the square brackets [ ] designate a calculated value.

3. Calculate $[T_{r_i}^{(0)}]$ by means of (9) using the results of step 2.

4. Compare the estimated $\{T_{r_i}^{(0)}\}$ against the computed $[T_{r_i}^{(0)}]$, relax the difference and recompute until

   $\{T_{r_i}^{(0)}\} - [T_{r_i}^{(0)}] \leq \varepsilon, \quad O(10^{-10})$

The values of $m_{i_1}^{(0)}$ and $m_{i_2}^{(0)}$ are derived from measurements of the SGC. For example, one may assume following Squires (1976) that each Al_2O_3 particle adsorbs a monomolecular

layer of HCl, leaving the HCl residue as vapor to be equilibrated with the condensing H_2O coating on each particle. The role of the adsorbed HCl in determining molality of the aquaeous phase may be modeled in various ways (i.e., assuming some proportion of solution and some residual adsorption bonding) in the absence of hard data. We depend upon our chemical advisers for aid in designing this part of the model.

b. Subsequent Time Steps

For subsequent time steps, $t^{(k)} = t^{(0)} + \Delta t^{(0)} + \Delta t^{(1)} + \ldots + \Delta t^{(k-1)}$, we calculate $dT_a^{(k)}/dt$ using equation (13). For values of dx_1/dt and dx_2/dt we use those determined from the prior time step. To compute $dT_a^{(0)}/dt$ we set

$$\frac{dx_1^{(-1)}}{dt} = \frac{dx_2^{(-1)}}{dt} = 0$$

For the droplet growth computations we define the parameter ψ

$$\psi^{(k-2)} = \frac{(T_r-T_a)^{(k-1)} - (T_r-T_a)^{(k-2)}}{\Delta t^{(k-2)}} \qquad (14)$$

and use it to predict $\{(T_r-T_a)^{(k)}\}$ by means of

$$\{(T_r-T_a)^{(k)}\} = (T_r-T_a)^{(k-1)} + \psi^{(k-2)}\ \Delta t^{(k-1)} \qquad (15)$$

For $k = 1$, we define $\psi^{(-1)} = 0$. This is equivalent to setting

$$\{(T_r-T_a)^{(1)}\} = (T_r-T_a)^{(0)}$$

which is a reasonable first estimate. The steps 2, 3, and 4 (see above: a. Initialization) are repeated to obtain the final values of $T_r^{(k)}$ and $dm_{1,2}{}^{(k)}/dt$.

5. Numerical Procedure

The predictor-corrector method of Hamming (Ralston and Wilf, 1960) is used for general integration of the explicit model at present. This technique does not "self-start"; so a fourth order Kutta-Simpson procedure is used through the first two time-steps. Although it is quite likely that more efficient procedures may be applied, our present orientation is toward generating a working model. We expect to take up the computational efficiency question separately at a later date.

6. Verification

Examination of the model derivations indicates that (a) the assumptions and approximations used to obtain the implicit droplet growth equation should lead to slightly lower than true growth rates; (b) the explicit equations should produce faster growth rates than the implicit equation gives, but their relation to the "true" growth rates is not easily judged.

Inasmuch as both systems can be applied to water condensation upon nuclei composed of inorganic salt, we have modeled the early stages of cloud droplet growth by each model using identical nuclei spectra and external conditions. The results for ammonium sulfate nuclei are shown in Fig. 2.1 for a steady updraft of 1 m sec^{-1} to a height of 100 m above cloud base. Here the explicit model gives slightly larger droplets than the implicit model

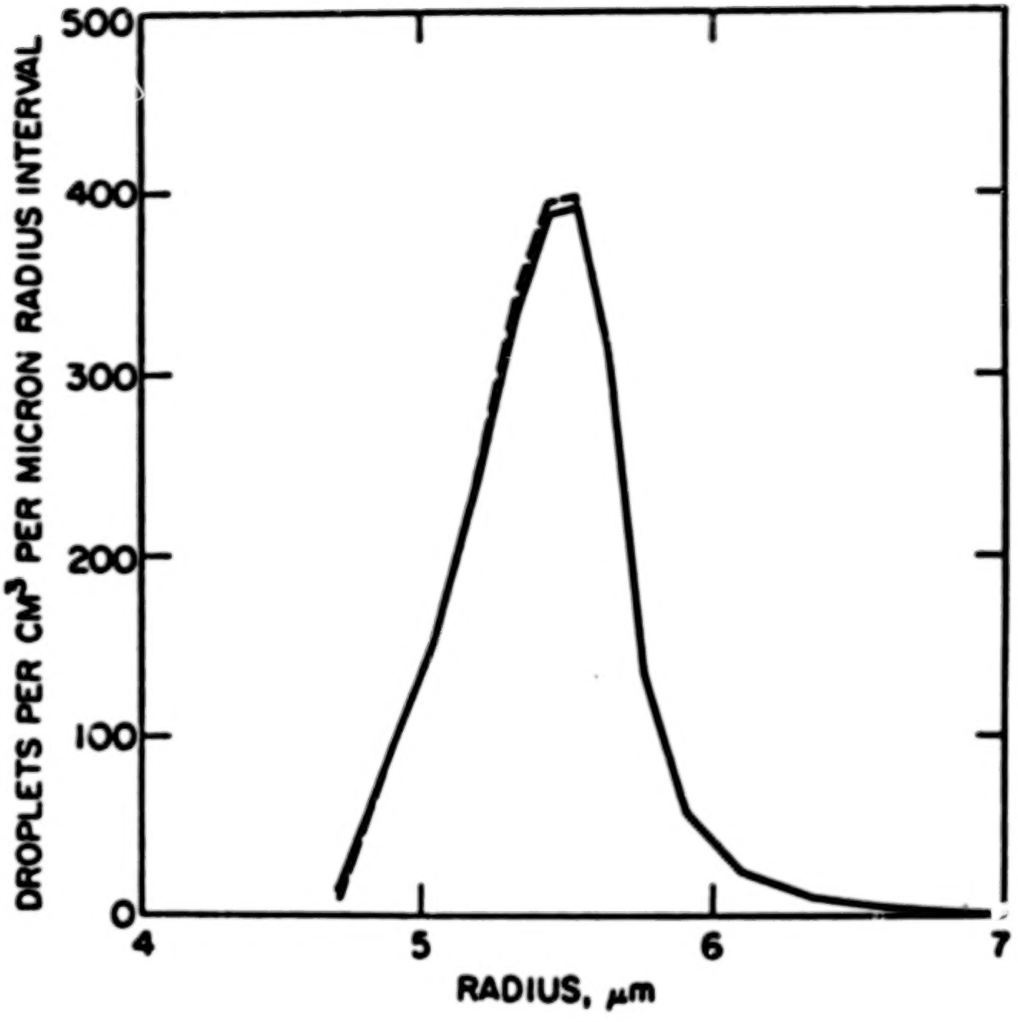

Fig. 2.1: Droplets per cm^3 per Micron Radius Interval-100 meters above cloud base, steady updraft.

Figure 2.2 shows results from both models for a simulated parcel trajectory that rose 20 m above cloud base at 1 m sec^{-1}, then returned to cloud base at 1 m sec^{-1} and rose again at this same rate to 100 m above cloud base. The nuclei again are ammonium sulfate, and both models give a bimodal distribution after 140 sec. The greater differences of size between the explicit and implicit model results is attributed partly to the longer time interval and partly to the failure of droplets smaller than the fourth size category to reactivate after the 20m-amplitude vertical displacement cycle in the explicit model calculations. During the second upward displacement, the saturation ratio does not achieve as large a value as during the first because the presence of the larger sized droplets provides an increased vapor sink as the second uplift stage begins.

We conclude that the explicit computations are adequately validated by the above for $(NH_4)_2SO_4$ nuclei. Additional tests are planned for salts having larger values of the heat of solution. NaOH, KOH and $KClO_4$ appear to be likely candidates for these computations.

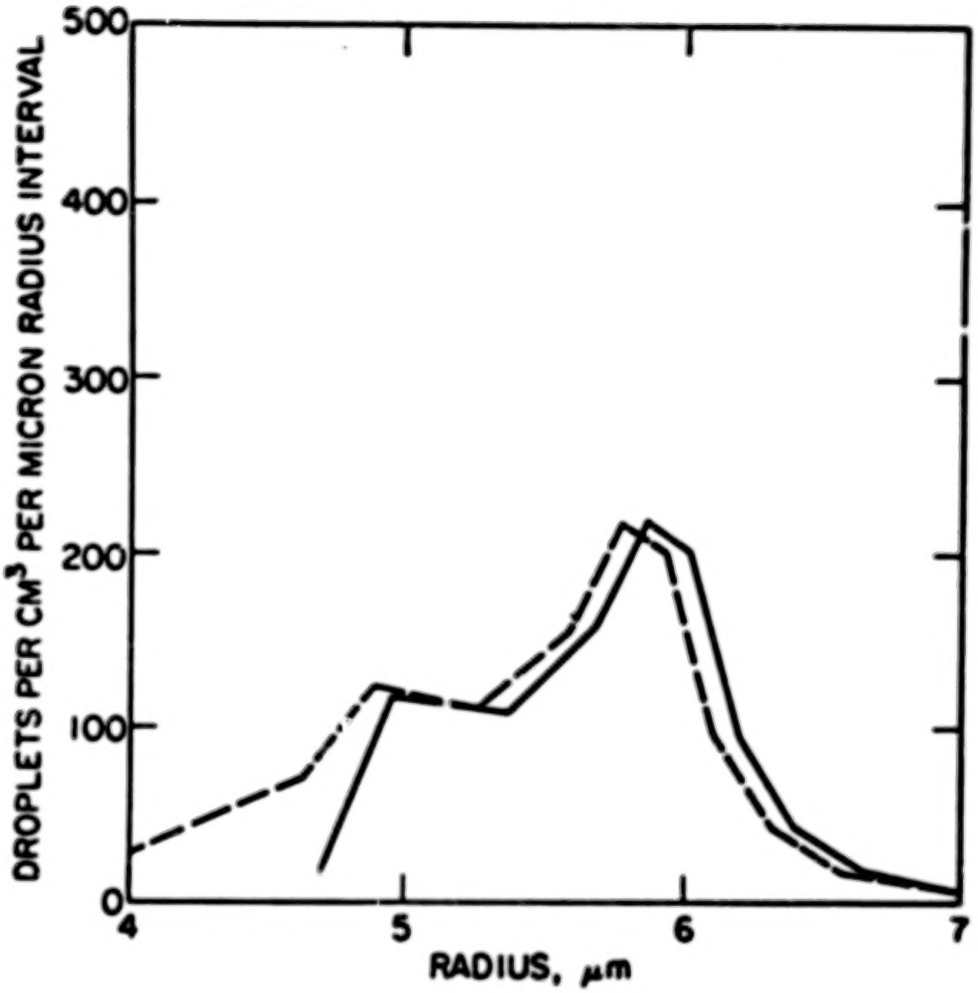

Fig. 2.2: Droplets per cm^3 per Micron Radius Interval-100 meters above cloud base, turbulent motion.

REFERENCES

Frössling, (1938): Über die Verdunstung fallen der Tropfen Beitrage Geophysik 52, 170.

Fuchs, N.A.,(1959): Evaporation and Droplet Growth in Gaseous Media, Pergamon, New York, 87 pp.

Mason, B.J., (1957): The Physics of Clouds, Oxford University Press, London, 481 pp.

Ralston, A., and H.S. Wilf, (1960): Mathematical Methods for Digital Computers, John Wiley and Sons, Inc., New York, 293 pp.

Squires, P., (1952): The growth of cloud drops by condensation, I. General characteristics, Austral. J. Sci. Res. A, 5, 59.

Squires, P.,(1976): Chap. IV of V. Mohnen, et.al., Report on Inadvertent Weather Modification Implications of the Stabilized Ground Cloud. Institute on Man and Science, Rensselaerville, New York, dated August 1976.

Weast, R.C., (1970): Handbook of Chemistry and Physics, 51st Edition, The Chemical Rubber Co., Clevelend, Ohio.

III. Meso-Scale Model

A. Introduction

A meso-scale meteorological model is being developed to study the diurnal and seasonal variations of the meso-scale weather patterns in the lower atmosphere over the Florida Peninsula. The basic structure of the model follows the work of Pielke (1974). We have introduced modifications for the purpose of removing some of the approximations of the original model. In particular parameterized effects of cloud and precipitation processes are introduced, and the boundary-layer processes are treated in more detail than in Pielke's three-dimensional model. Nonetheless, these processes are still highly parameterized, because they cannot be resolved explicitly in the meso-scale. The detailed formulations of this model are presented in the following sections.

The results from this model will be used as continuous inputs to a sub-meso-scale model for the area of Cape Canaveral to predict the processes and patterns of SRM exhaust product removal after Space Shuttle launches.

B. Basic Equations

Several basic assumptions are made in deriving the system of equations that express the atmospheric processes. They are

(1) that the ideal gas law is valid for moist air, i.e.

$$p = \rho R T_v$$

(2) that the shallow atmosphere has constant density, i.e.

$$\frac{d\rho}{dt} = 0$$

and

(3) that a hydrostatic balance is held for the meso-scale motions, i.e.

$$\frac{\partial p}{\partial z} = - \rho g,$$

where p is the pressure, ρ the density, T_v the virtual temperature, R [illegible] specific gas constant for the air and g the gravitational acceleration.

After performing the scale analysis, the basic equations in Cartesian coordinates for the meso-scale motion are,

$$\frac{du}{dt} = - \frac{1}{\rho} \frac{\partial p}{\partial x} + fv - f_* w + F_u \qquad (2.1)$$

$$\frac{dv}{dt} = - \frac{1}{\rho} \frac{\partial p}{\partial y} - fu + F_v \qquad (2.2)$$

$$- \frac{1}{\rho} \frac{\partial p}{\partial z} = \rho g \qquad (2.3)$$

$$\frac{\partial u}{\partial x} + \frac{\partial v}{\partial y} + \frac{\partial w}{\partial z} = 0 \qquad (2.4)$$

$$p = \rho R T_v \qquad (2.5)$$

$$\frac{d\theta}{dt} = \frac{\theta}{c_p T}(S_\theta + F_\theta) \qquad (2.6)$$

$$\frac{dq}{dt} = S_q + F_q \qquad (2.7)$$

where

$$\frac{d}{dt}(i) = \left(\frac{\partial}{\partial t} + u\frac{\partial}{\partial x} + v\frac{\partial}{\partial y} + w\frac{\partial}{\partial z}\right)(i)$$

$$F_{(i)} = \left[\frac{\partial}{\partial x}\left(K_H \frac{\partial(i)}{\partial x}\right) + \frac{\partial}{\partial y}\left(K_H \frac{\partial(i)}{\partial y}\right) + \frac{\partial}{\partial z}\left(K_z^{(i)} \frac{\partial(i)}{\partial z}\right)\right]$$

$$f = 2\Omega \sin\phi,$$

$$f_* = 2\Omega \cos\phi,$$

u, v, and w are the x-, y-, and z- components of velocity respectively, θ the potential temperature, q the specific humidity, Ω the earth rotation rate, and ϕ the latitude. K_H and $K_z^{(i)}$ are the horizontal and vertical eddy exchange coefficients. K_H has the following form (Leith, 1969):

$$K_H = C_o(\Delta x)(\Delta y)\left\{\left(\frac{\partial v}{\partial y} + \frac{\partial u}{\partial y}\right)^2 + 1/2\left[\left(\frac{\partial u}{\partial x}\right)^2 + \left(\frac{\partial v}{\partial y}\right)^2\right]\right\}^{1/2}$$

where C_o is a constant, Δx and Δy are the x- and y- direction grid spacing. $K_z^{(i)}$ is defined below (section 6) in the discussion of the boundary-layer parameterization. S_θ and S_q are the source functions respectively for the potential temperature and the specific humidity. The details can be found below in section 5 on cloud and precipitation parameterization.

Now we introduce two dependent variables. First, the non-dimenaional pressure (π) has the following definition,

$$\pi = c_p(p/p_*)^{R/c_p} \qquad (2.8)$$

where c_p is the specific heat capacity at constant pressure, and p_* (=1000 mb) the reference pressure. Secondly the

virtual potential temperature (θ_v) is defined,

$$\theta_v = T_v(p_*/p)^{R/c_p} = \frac{T_v}{c_p}\,\pi \qquad (2.9)$$

Using (2.5), (2.8), and (2.9), the pressure gradient terms, which appear in (2.1), (2.2), and (2.3) become

$$-\frac{1}{\rho}\frac{\partial p}{\partial x} = -\theta_v\frac{\partial \pi}{\partial x}$$

$$-\frac{1}{\rho}\frac{\partial p}{\partial y} = -\theta_v\frac{\partial \pi}{\partial y}\ , \text{ and}$$

$$-\frac{1}{\rho}\frac{\partial p}{\partial z} = -\theta_v\frac{\partial \pi}{\partial z}\ .$$

Introducing these expressions, the basic equations may be rewritten as follows:

$$\frac{du}{dt} = -\theta_v\frac{\partial \pi}{\partial x} + fv = f_*W + Fu \qquad (2.10)$$

$$\frac{dv}{dt} = -\theta_v\frac{\partial \pi}{\partial y} - fu + F_v \qquad (2.11)$$

$$\frac{\partial \pi}{\partial z} = \frac{g}{\theta_v} \qquad (2.12)$$

$$\frac{\partial w}{\partial z} = -\left(\frac{\partial u}{\partial x} + \frac{\partial v}{\partial y}\right) \qquad (2.13)$$

$$\frac{d\theta}{dt} = \frac{1}{\pi}(S_\theta + F_\theta) \qquad (2.14)$$

$$\frac{dq}{dt} = S_q + F_q \qquad (2.15)$$

and

$$\theta_v = \theta(1 + 0.609q) \qquad (2.16)$$

C. Boundary Conditions:

To eliminate reflection from the boundaries, and to have smooth continuation of the flow through the boundaries, the following boundary conditions are assumed:

(1) Lateral boundaries:

$$\frac{\partial u}{\partial x} = \frac{\partial v}{\partial x} = \frac{\partial \theta_v}{\partial x} = \frac{\partial q}{\partial x} = 0 \qquad \text{at } x = 0, \text{ and } L_1;$$

$$\frac{\partial u}{\partial x} = \frac{\partial v}{\partial y} = \frac{\partial \theta_v}{\partial y} = \frac{\partial q}{\partial y} = 0 \qquad \text{at } y = 0, \text{ and } L_2 ,$$

where L_1 and L_2 are the lengths of the horizontal model region in x- and y- direction respectively.

(2) Bottom boundary:

The bottom surface is flat, and $u = v = w = 0$. The virtual potential temperature (θ_v) and the specific humidity (q) are determined by time-dependent functions which simulate the diurnal variation and also imply solar and nocturnal radiations. These functions are expressed by truncated Fourier series. They operate to perturb the initial balanced state and indirectly to generate the meso-scale motion.

D. Initial Conditions

The following data are needed to initiate the model:

(1) a three-dimensional moisture field,

(2) a three-dimensional temperature field, and

(3) a two-dimensional surface pressure field.

The specific humidity, q, is derived from dew-point, temperature and pressure data. The virtual potential temperature and the non-dimensional pressure are calculated by (2.8), (2.9), and (2.12).

The initial horizontal velocity field is determined on the basis of two assumptions; first, that the lowest 5 levels in the model are assumed to have the Ekman solutions (Holton, 1972), and, second, that geostrophic balance prevails at the higher levels. The initial vertical velocity is computed by (2.13).

The initial height of the top free surface is given by

$$h = (p_{sfc} - p_h)/\rho g,$$

where p_{sfc} is the surface pressure, and p_h = 500 mb.

B. Cloud and Precipitation Parameterization.

The effect of latent heat release from clouds and precipitation upon the meso-scale motion is parameterized into two major parts. This allows the source terms in (2.14) and (2.15) to be expressed by

$$S = S_{\theta_1} + S_{\theta_2}, \text{ and} \tag{5.1}$$

$$S_q = S_{q_1} + S_{q_2} \tag{5.2}$$

where subscripts 1 and 2 denote stable and convective precipitation respectively.

(1) Stable precipitation

By assuming that the stable precipitation process is pseudo-adiabatic, S_{θ_1} and S_{q_1} may be written in the form:

$$S_{\theta_1} = \begin{cases} -L\, dq_s/dt, & \text{when } q>q_s \text{ and } w>0, \\ 0, & \text{when } q\leq q_s \text{ or } w\leq 0 \end{cases} \qquad (5.3)$$

$$S_{q_1} = \begin{cases} dq_s/dt, & \text{when } q>q_s \text{ and } w>0, \\ 0, & \text{when } q\leq q_s \text{ or } w\leq 0 \end{cases} \qquad (5.4)$$

where q_s is the saturation specific humidity, and L the latent heat of condensation.

The rate of change of q_s is given by

$$\frac{dq_s}{dt} = \frac{q}{\varepsilon} \left(\frac{c_p T - \varepsilon L}{c_p R_v T^2 + q_s L^2}\right) q_s w \qquad (5.5)$$

where $\varepsilon = 0.622$, and R_v is the gas constant for water vapor. The detailed derivation can be found in Haltiner (1970) with minor transformation to adapt to the present coordinate system.

(2) Convective precipitation.

The parameterization of convective precipitation for larger scales has been organized by Fraedrich (1973) using the concepts of compensating subsidence (Arakawa, 1971) and of lateral mixing (Kuo, 1965). The source terms for θ and q are

$$S_{\theta_2} = mc_p(\Gamma_d - \Gamma) + (1-\alpha)\rho c_p a(T_c - T)/\Delta t, \qquad (5.6)$$

and

$$S_{q_2} = m \frac{\partial q}{\partial z} + a[(q_c - q) + \alpha \frac{c_p}{L} (T_c - T)]/\Delta t \qquad (5.7)$$

where m(z) is the vertical mass flux, Γ_d the dry adiabatic process rate, Γ the environmental lapse rate, a the fraction of a horizontal grid area covered by convective cloud, and α the ratio of evaporation to condensation. The subscript c denotes saturated values on the moist adiabat through the cloud base and Δt is the time step of the numerical integration scheme.

The vertical mass flux m(z) can be determined by an entrainment function suggested by Fraedrich (1973),

$$\frac{1}{m(z)} \frac{\partial m(z)}{\partial z} = \frac{0.4}{D_c} \qquad (5.8)$$

where D_c is the cloud diameter, and it is linearly related to cloud depth (z_0) (Plank, 1969-; Belts, 1973), i.e.

$$\frac{D_c}{z_0} \sim 1. \qquad (5.9)$$

The fraction, a, of the grid area covered by convective cloud is the ratio,

$$a = \frac{C_1}{C_2 + C_3} \quad . \qquad (5.10)$$

Here C_1 is the total integrated horizontal moisture convergence in the layer between the cloud base (z_B) and the level (z_T) where the moist adiabat through the cloud base intersects the environment sounding, plus the surface evaporation, that is

$$C_1 = \Delta T \{ - \int_{z_B}^{z_1} \rho [\frac{\partial}{\partial x}(qu) + \frac{\partial}{\partial y}(qv)]dz + E_v \} , \qquad (5.11)$$

where

$$E_v = \rho C_D V_o (q_w - q_o) \qquad (5.12)$$

C_D is the drag coefficient, V_o the wind speed at the level just above the surface, q_w the specific humidity at the underlying surface, and q_o the specific humidity at the level just above the surface.

C_2 and C_3 are expressed by

$$C_2 = \int_{z_B}^{z_T} \rho (q_c - q)dz, \text{ and} \qquad (5.13)$$

$$C_3 = \int_{z_B}^{z_T} \rho \frac{c_p}{L}(T_c - T)dz. \qquad (5.14)$$

The sum of C_2 and C_3 represents the total water vapor that can be condensed.

Finally, the weighting factor α is the ratio of evaporation to condensation, and $(1-\alpha)$ is the ratio of rainfall to condensation.

F. Boundary-Layer Parameterization

The atmosphere below 500 mb in this model is divided into three physical layers. They are (1) the surface boundary layer (SBL), (2) the planetary boundary layer (PBL) and (3) the free atmosphere layer. The SBL is a constant flux layer attached directly to the surface. The PBL is immediately above the SBL, and the region above the PBL is the free atmosphere. The atmosphere above 500 mb is assumed to be stable.

The vertical eddy exchange coefficient, $K_z^{(i)}$ which appears in equations (2.1, 2.2, 2.6 and 2.7) may be assumed to be a function of z. Because of the different stability conditions between daytime and nighttime, it is difficult to formulate a universal function to represent a full diurnal cycle. For daytime, the formulae in O'Brien (1970) are adopted; for nighttime, a functional expression is being developed.

A summary of the vertical profile of $K_z^{(i)}$ in the daytime is given as follows,

$$K_z^{(i)} = \begin{cases} K_1^{(i)} + [(H_*-z)^2/(H_*-h_*)^2]\{(K_2^{(i)}-K_1^{(i)}) + \\ (z-h_*)[K_3^{(i)} + 2\,(K_2^{(i)}-K_1^{(i)})/(H_*-h_*)]\}, & \text{for } h_* \le z \le H_* \\ K_1^{(i)}, & \text{for } H_* < z \\ (z/h_*)K_2^{(i)}, & \text{for } z < h_* \end{cases} \tag{6.1}$$

where $K_1^{(i)}$ and $K_2^{(i)}$ are the values of $K_z^{(i)}$ at H_*, the altitude at the top of the PBL, and at h_*, the altitude at the top of the SBL, respectively,

$$K_3^{(i)} = \left(\frac{\partial K_z^{(i)}}{\partial z}\right)\Big|_{h_*} \tag{6.2}$$

and superscript i can be momentum, potential temperature, or specific humidity. $K_1^{(i)}$ is a constant in the free atmosphere. A Hermite interpolating polynomial suggested by O'Brien (1970) determines the distribution of $K_z^{(i)}$ in the PBL. In the SBL, $K_z^{(i)}$ is a linear function of z.

H_* is given by a time-dependent, empirical equation introduced by Deardorff (1974),

$$\frac{\partial H_*}{\partial t} = -\left(u \frac{\partial H_*}{\partial x} + v \frac{\partial H_*}{\partial y}\right) + w_i^* + \frac{1.8(w_*^3 + 1.1U_*^3 - 3.3U_* f H_*)}{g \frac{H_*^2}{\theta_v} \left(\frac{\partial \theta_v}{\partial z}\right)_{H_*} + g w_*^2 + 7.2U_*^2} \tag{6.3}$$

where

$$w_i^* = a w_* + (1-a)w, \tag{6.4}$$

$$w_* = \begin{cases} \left(-\frac{g}{\theta_v} U_* \theta_* H_*\right)^{-1/3}, & \text{if } \theta_* \leq 0; \\ 0, & \text{if } \theta_* > 0, \end{cases} \tag{6.5}$$

and $\left(\frac{\partial \theta_v}{\partial z}\right)_{H_*}$ is the virtual potential temperature gradient at H_*, and U_* and θ_* are defined below.

A relation between H_* and h_* is given by Pielke (1974), and Pielke and Mahrer (1975) based on the work of Blackadar and Tennekes (1968). That is

$$h_* = 0.04 \, H_* \tag{6.6}$$

$K_2^{(i)}$ is determined by the micro-meteorological processes in the SBL. It is evaluated by means of the empirical expressions derived by Businger (1973), on the basis of relatively recent field data (Businger, et.al. 1971). $K_2^{(i)}$ has the following forms.

$$K_2^{(m)} = k U_* h_* / \phi_M \tag{6.7}$$

$$K_z^{(\theta)} = K_z^{(q)} = kU_* h_* / \phi_H \tag{6.8}$$

where k is the von Karman constant. The dimensionless wind shear

$$\phi_M = \frac{kz}{U_*} \frac{\partial U}{\partial z} , \tag{6.9}$$

where

$$U = (u^2 + v^2)^{1/2}$$

and where the dimensionless virtual potential temperature gradient

$$\phi_H = \frac{z}{\theta_*} \frac{\partial \theta_v}{\partial z} \tag{6.10}$$

have been fitted to real observational data by Businger et.al. (1971). The empirical functions for them are,

$$\phi_M = \begin{cases} (1-15\xi)^{-1/4}, & \xi \leq 0, \\ 1+4.7\xi, & \xi > 70, \end{cases} \tag{6.11}$$

and

$$\phi_H = \begin{cases} 0.74\ (1-9\xi)^{-1/2}, & \xi \leq 0, \\ 0.74 + 4.7\xi, & \xi > 0, \end{cases} \tag{6.12}$$

where $$\xi = z/L, \tag{6.13}$$

$$L = \bar{\theta}_v / g(U_*^2 / kz\theta_*) , \tag{6.14}$$

U_* is the friction velocity, and θ_* the scaling potential temperature. After integrating (6.9) and (6.10) with respect to z, we have

$$U_* = kU|_{h^*} / [\ell n(z/z_o) - \psi_1] \tag{6.15}$$

and

$$\theta_* = [\theta_v|_{h_*} - \theta_{v\ sfc}]/[0.74\ \ln(z/z_o) - 0.74\psi_2], \qquad (6.16)$$

where

$$\psi_1 = \begin{cases} 2\ \ln[(1+\phi_M^{-1})/2] + \ln[(1+\phi_M^{-2})/2] - 2\tan^{-1}(\phi_M^{-1}) + \pi/2, & \xi \leq 0, \\ -4.7\xi, & \xi > 0, \end{cases} \qquad (6.17)$$

$$\psi_2 = \begin{cases} \ln[(1+0.74\phi_H^{-1})/2], & \xi \leq 0 \\ 0.74 + 4.7\xi & \xi > 0 \end{cases} \qquad (6.18)$$

$U|_{h_*}$ is the wind velocity at h_*, $\theta_v|_{h_*}$ and $\theta_v|_{sfc}$ are θ_v at h_* and at surface respectively, z_o is the roughness length which is different between water and land surfaces. Over water,

$$a_o = 0.032\ U_*^2/g \qquad (6.19)$$

suggested by Clarke (1970) is used, whereas over land it is assumed constant (4 cm in this model).

In order to close the system described above, one must know ξ. The formulation of ξ involves the Richardson number Ri, which is defined by,

$$Ri = \frac{g}{\bar{\theta}_v} \frac{\frac{\partial \theta_v}{\partial z}}{(\frac{\partial U}{z})^2} \qquad (6.20)$$

in the SBL, where $\bar{\theta}_v$ is the average virtual potential temperature, $\frac{\partial \theta_v}{\partial z}$ the virtual potential temperature gradient, and $\frac{\partial U}{\partial z}$ the wind shear. With the aid of (6.9), (6.10), (6.13), and (6.14) we get an analytic relation,

$$Ri = \frac{\phi_H(\xi)}{\phi_M^2(\xi)} \tag{6.21}$$

Substituting (6.11), and (6.12) into (6.21) we have an algebraic equation for ξ,

$$a_*\xi^3 + b_*\xi^2 + c_*\xi + d_* = 0 \tag{6.22}$$

where

$$\left.\begin{aligned} a_* &= -8.214 \\ b_* &= 0.5476 \\ c_* &= 9Ri^2 \\ d_* &= -Ri^2 \end{aligned}\right\} \text{for } Ri \leq 0$$

and

$$\left.\begin{aligned} a_* &= 0 \\ b_* &= 22.09Ri=4.7 \\ c_* &= 9.4Ri-0.74 \\ d_* &= Ri^2 \end{aligned}\right\} \text{for } Ri>0$$

The Richardson number in the present boundary-layer parameterization will be approximated by a quasi-local version of the Richardson number ($\overline{Ri}$) suggested by Portman (1974),

$$\overline{Ri} = [2gz_{1,2}(\theta_{v2}-\theta_{v1}) \ln n_*]/[\overline{\theta_v} (U_2-U_1)^2], \tag{6.23}$$

where

$$z_{1,2} = (h_* z_o)^{1/2}$$

$$n_* = h_*/z_o,$$

and subscripts 1, and 2 denote the values at h_* and z_o, respectively.

For the nighttime, the formulation for $K_z^{(i)}$ is being investigated, and will be presented later.

6. Numerical Methods

(1) Model structure

A horizontal area (720 km x 480 km) is chosen to cover the Florida Peninsula in the center and the surrounding water (Figure 3.1). The horizontal grid-space ($\Delta x = \Delta y$) is 30 km. Study of grid spacing down to 15 km will be conducted to evaluate the effect of this parameter. The atmosphere below 500 mb will be divided vertically into ten levels with spacing (Table 3.1). The time increment (Δt) will depend on the computational criterion of the numerical scheme used.

(2) Numerical schemes

The differential equations shown in the previous sections will be approximated by the algebraic difference equations using finite-difference methods. The total derivative with respect to any dependent variable, A,

$$\frac{dA}{dt} = \frac{\partial A}{\partial t} + u\frac{\partial A}{\partial x} + v\frac{\partial A}{\partial y} + w\frac{\partial A}{\partial z} \qquad (7.1)$$

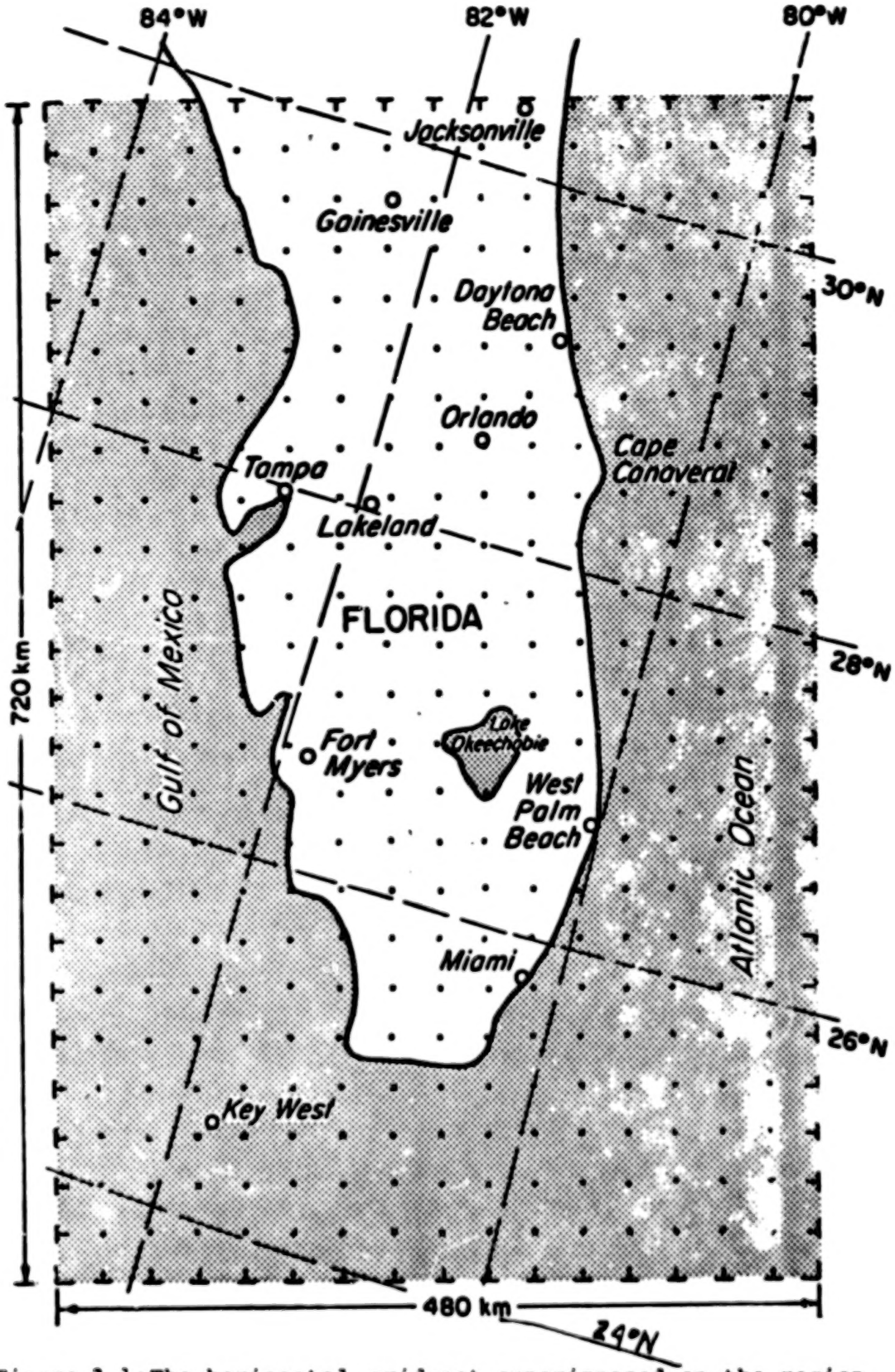

Figure 3.1: The horizontal grid-net superimposed on the region of simulation in the meso-scale model.

Table 3.1

Height of Fixed Vertical Level

Level No.	Height (km)
11	5.00
10	4.05
9	3.20
8	2.45
7	1.80
6	1.25
5	0.80
4	0.45
3	0.20
2	0.05
1	0.00

will be approximated by the forward-upstream scheme (Molenkamp, 1968). It can be expressed as

$$\left(\frac{dA}{dt}\right)^n_{ijk} = \frac{1}{\Delta t}(A^{n+1}_{ijk} - A^n_{ijk}) + (P^n_{ijk} + Q^n_{ijk} + R^n_{ijk}), \qquad (7.2)$$

where

$$P^n_{ijk} = \begin{cases} u^n_{ijk}(A^n_{ijk}-A^n_{i-1,jk})/\Delta x, & u^n_{ijk} > 0 \\ u^n_{ijk}(A^n_{i+1,jk}-A^n_{ijk})/\Delta x, & u^n_{ijk} \leq 0 \end{cases}$$

$$Q^n_{ijk} = \begin{cases} v^n_{ijk}(A^n_{ijk}-A^n_{i,j-1,k})/\Delta y, & v^n_{ijk} > 0 \\ v^n_{ijk}(A^n_{i,j+1,k}-A^n_{ijk})/\Delta y, & v^n_{ijk} \leq 0 \end{cases}$$

$$R^n_{ijk} = \begin{cases} w^n_{ijk}(A^n_{ijk}-A^n_{i,j,k-1})G(k), & w^n_{ijk} > 0 \\ w^n_{ijk}(A^n_{ij,k+1}-A^n_{ijk})G(k). & w^n_{ijk} \leq 0 \end{cases}$$

In (7.2) the subscripts i, j, and k represent the location of the grid points in the model,

$$x = (i-1)\Delta x$$

$$y = (j-1)\Delta y$$

$$z = G(k)$$

where G(k) is a function to space the uneven vertical levels. The superscript n shows the number of the time step,

$$T = n\Delta t.$$

All other terms in the differential equations will be computed using the central-difference scheme.

The computational criterion for the forward-upstream scheme is

$$\left|\frac{V_* \Delta t}{\Delta}\right| < 1$$

where V_* is the maximum speed of any component of velocity and Δ the corresponding grid spacing.

REFERENCES

Arakawa, A., 1972: Design of the UCLA general circulation model. Numerical Simulation of Weather and Climate, Tech. Report No. 7., Department of Meteorology, UCLA, 116 pp.

Belts, A.K., 1973: A relationship between stratification, cloud depth, and permitted cloud radii. J. Appl. Meteor., 12, 890-893.

Blackadar, A.K., and H. Tennekes, 1968: Asymptotic similarity in neutral barotropic planetary boundary layers. J. Atmos. Sci., 25, 1015-1020.

Businger, J.A., 1973: Turbulent transfer in the atmospheric surface layer. Workshop on Micrometeorology, Amer. Meteor. Soc., Chap. 2, 67-100.

Businger, J.A., J.C. Wyngaard, Y. Izami, and E.F. Bradley, 1971: Flux-profile relationships in the atmospheric surface layer. J. Atmos. Sci., 28, 181-189.

Clarke, R.H., 1970: Recommended methods for the treatment of the boundary layer in numerical models. Australian Meteor. Mag., 18, 51-73.

Deardorff, J., 1974: Three-dimensional numerical study of the height and mean structure of a heated planetary boundary layer. Boundary Layer Meteor., 7, 81-106.

Fraedrich, K., 1973: On the parameterization of cumulus convection by lateral mixing and compensating subsidence. Part I. J. Atmos. Sci., 30, 408-413.

Haltiner, G.J., 1971: Numerical Weather Prediction. John Wiley & Sons, New York, New York, 317 + xvi pp.

Holton, J.R., 1972: An Introduction to Dynamic Meteorology. Academic Press, New York, New York, 319 + xi pp.

Kuo, H.L., 1965: On formation and intensification of tropical cyclones through latent heat release by cumulus convection. J. Atmos. Sci., 22, 40-63.

Leith, C.E., 1969: Two dimensional eddy viscosity coefficients. Proc. WMO/IUGG Symp. on Num. Wea. Pre. in Tokyo, Nov. 26-Dec. 4, 1968. Japan Meteorological Agency, Tokyo, 141-144.

Molenkamp, C.R., 1968: Accuracy of finite-difference methods applied to the advection equation. J. Appl. Meteor. 7, 160-167.

O'Brien, J.J., 1970: A note on the vertical structure of the eddy exchange coefficient in the planetary boundary layer. J. Atmos. Sci., 27, 1213-1215.

Pielke, R.A., 1974: A three-dimensional numerical model of the sea breezes over south Florida. Mon. Wea. Rev. 102, 115-139.

Pielke, R.A., and Y. Mahrer, 1975: Representation of the heated planetary boundary layer in mesoscale models with coarse vertical resolution. J. Atmos. Sci., 32, 2288-2308.

Plank, V.G., 1969: The size distribution of cumulus clouds in representative Florida populations. J. Appl. Meteor., 8, 46-47.

Lettau, H.H., 1957: Computation of Richardson numbers, classification of wind profiles, and determination of roughness parameters. In Exploring the Atmosphere's First Mile, Vol. 1, Instrumentation and Data Evaluation, Ed. by H.H. Lettau and B. Davidson, Pergamon Press, New York, 328-336.

IV. Input Data on Equilibrium Vapor Pressures for HCl and H_2O over HCl_{aq}

Basic to the microphysical model calculations for the two volatile components, HCl and H_2O, is the information on equilibrium concentrations of these vapors over HCl_{aq}. For our purpose, it is important that the data reflecting these concentrations provide for the ranges of temperature and molality that are likely to be encountered in tropospheric cloud formation. It is a simple matter of circumstance that most chemical measurements available in the literature and handbooks have not been made with atmospheric applications in view. In this case, the best available data are those of Fritz and Fuget (1956) which give vapor pressures over bulk HCl_{aq} for H_2O vapor and HCl vapor equilibria in the range of temperature $273°K \leq T \leq 323°K$ and for solution molality ranging from 0 to 15.88.

Although initially, in dealing with the stabilized ground cloud (estimated altitude below 1 km) and the stabilized column cloud (altitude up to 3 km) over Florida, the temperatures to be encountered should not go much below 263°K, we have the further consideration of ingestion into active convective cells in which much greater height and temperatures down to 243°K or colder may be encountered. Thus it is necessary to extend the tabulated data of Fritz and Fuget (l.c.) beyond the limit of the measurements.

An additional requirement upon these data for use in numerical modeling is that they form a smooth and continuous

functional surface throughout the domains of the data. In general, even with the best of experimental work, normal experimental error and accidental mistakes become incorporated into the results. It is a problem of statistical curve fitting and analysis of variance to (a) discover "out-rider" values in such sets of data, so that they can be charged to "mistakes" and deleted so as to prevent an undue influence of these values upon the smoothing process, and (b) to formulate best-fit smooth functional curves, calculated to minimize the sum of squares of the departures of the measured data points from the calculated (fitted) curves.

In the present instance, an additional requirement upon the curve-fitting analysis is that it provides the best possible curve forms for use in extending the domain beyond that of the measurements. This is in no way to be construed as being equivalent to making measurements in the domain extension: it is only an approximation technique that links the estimated values in the non-measured region as firmly as possible to the measured values. The need for suitable laboratory measurements on HCl_{aq} at temperatures below 273°K is thus emphasized, not met, by the present effort.

A. Form of Curves

Particularly in the event that extrapolations are required, it is basic that statistical curve fitting be guided by physical theory. The form of the dependency of vapor pressure on temperature for pure vapors in equilibrium with their liquid or solid phases is indicated by the Clausius-Clapeyron relation.

$$\frac{dp}{dT} = \frac{L}{R_v} \frac{p}{T^2} \tag{1}$$

Although L, the latent heat associated with the phase transition is quite constant, it can be shown that, if the vapor behaves approximately as an ideal gas, L depends upon T

$$L = L_o + \ell T, \quad \ell = \Delta c_p = c - c_{pv} \tag{2}$$

where c is the specific heat of the liquid or solid phase and c_{pv} is the specific heat at constant pressure of the vapor. Hence the definite integral of (1) over a temperature interval gives an equation of the form

$$\ln p]_\mu = A + BT^{-1} + C \ln T \tag{3}$$

for solutions of constant molality, μ.

The dependency of the equilibrium vapor pressure upon concentration is indicated for constant temperature by Raoult's Law to have the form

$$\ln p]_T = D + E\mu \tag{4}$$

To provide for departure from ideal conditions, the right side of this equation may be extended with terms in powers or other functions of μ (i.e., $\ln \mu$, $\exp \mu$, etc.). In the absence of physical reasons for specific choices, the statistical procedure of multivariate analysis permits selection of those functions that most directly reduce the sum of squares of the departures.

Obviously the vapor pressures in the present case are dependent upon both temperature and molality, hence they may most directly be expressed as a surface in (p,T,μ) space by means of the polynomial

$$\ln p = (A + BT^{-1} + C \ln T)(D + E_{\mu} + \ldots) \qquad (5)$$

In the present instance, however, the need to extrapolate values to negative Celsius temperatures is basic, and can be done most readily on the strength of the Clausius-Clapeyron relation (1) and (3).

B. Procedure

The water vapor pressure table was considered first using equation (3) for the basic form relating water vapor pressure and temperature at each HCl_{aq} concentration listed. The least squares curve fitting routine thus provided a set of curves:

$$\ln p_{H_2O}]_{\mu} = A_0 + B_0 \ln T + C_0 T^{-1}$$

which is most readily represented by the array of A_0, B_0, C_0 values:

A_{00}	B_{00}	C_{00}
A_{01}	B_{01}	C_{01}
A_{02}	B_{02}	C_{02}
.	.	.
.	.	.
.	.	.
A_{0i}	B_{0i}	C_{0i}

for $\mu_0 = 0, \mu_1, \mu_2 \ldots \mu_i$, respectively.

In the initial step of the analysis, the presence of outriders became evident. Three criteria were used to remove subjectivity from the decision to classify a value as an outrider and delete it from the input data: (a) the departure of the measured data point from the smooth p vs T curve derived by using all data for each μ-value; (b) the amount of reduction of the root mean square error of the fitted curve obtained by eliminating the suspect data point; and (c) the regularity of the variation of the coefficients A, B and C across the array. The following three points were classed as outriders and deleted as a result: μ = 8.0, T = 273°K; μ= 11.0, T = 273°K; and μ= 15.0, T = 313°K. Unfortunately two of these points are at the lower T-limit of the measured data, i.e., at the threshold of the region to be extrapolated. Results at molalities of 2.0 and 9.0 were relatively poor, but no single point qualified as an outrider according to the criteria cited above.

Table 4.1 gives the numerical values for the μ_i and the coefficients, and Figures 4.1, 4.2 and 4.3 show graphically the variations of the coefficients as functions of the molality.

There is no clear physical criterion for the behavior of the coefficients A, B and C as functions of μ. On the other hand, it appears that a non-smooth or discontinuous variation of these numbers with molality must be physically unrealistic. It is therefore appropriate to smooth $A(\mu)$, $B(\mu)$, and $C(\mu)$ using the least squares curve-fitting procedures described above. Inasmuch as $C(\mu)$ exhibits the least variability

Table 4.1: Numerical Values of the Coefficient A_0, B_0, C_0 for Molalities $0 \leq \mu \leq 15.88$

μ	A_0	B_0	C_0
0	54.413	-4.9977	-6789.2
0.05	52.489	-4.7118	-6701.8
0.10	52.729	-4.7478	-6712.7
0.20	52.262	-4.6793	-6690.8
0.50	52.228	-4.6749	-6691.1
1.0	46.635	-3.8416	-64 3.9
2.0	35.498	-2.1624	-5989.8
3.0	43.796	-3.4242	-6338.9
4.0	42.654	-3.2588	-6301.2
5.0	40.248	-2.9020	-6215.7
6.0	44.018	-3.4650	-6411.9
7.0	40.240	-2.9032	-6272.3
8.0	62.165	-6.1702	-7293.4
9.0	46.358	-3.8353	-6582.3
10.0	49.957	-4.3601	-6804.7
11.0	86.551	-9.8109	-8496.4
12.0	36.227	-2.3107	-6275.7
13.0	67.505	-6.9558	-7751.6
14.0	27.670	-1.0224	-5998.7
15.0	31.200	-1.5449	-6207.0
15.88	-55.010	11.424	-2569.8

(Figure 41) from a smooth curve, it was smoothed first leading to the revised function $C_1(\mu)$:

$$C_1(\mu) = -6753.4 + 363.79\mu - 66.826\mu^2 + 2.6591\mu^3 + 0.56202 \times 10^{-3} \exp(\mu).$$

New values $A_1(\mu)$ and $B_1(\mu)$ were then computed using $C_1(\mu)$ in conjunction with the measured data points, outriders deleted, and $B_1(\mu)$ was smoothed, giving a revised function $B_2(\mu)$:

$$B_2(\mu) = - 4.8693 + 1.2115\mu - 0.21394\mu^2 + 0.86707 \times 10^{-2}\mu^3 + 0.19812 \times 10^{-5} \exp(\mu).$$

Again new values $A_2(\mu)$ were computed using $C_1(\mu)$ and $B_2(\mu)$ in the regression calculation. Smoothing of these gave the revised function $A_3(\mu)$:

$$A_3(\mu) = 53.560 - 8.1475\mu + 1.4352\mu^2 - 0.058161\mu^3 - 0.13170 \times 10^{-4} \exp(\mu).$$

and the smoothed functions are used in

$$\ln p_{H_2O}(\mu,T) = A_3(\mu) + B_2(\mu) \ln T + C_1(\mu)T^{-1} \qquad (6)$$

to represent the entire water vapor pressure surface in (p,μ,T) space. Equation (6) predicts the $p_{H_2O}(\mu,T)$ values with an overall average error of 0.5 percent with respect to the tabulated data points. The greatest error of 3.22 percent occurs at $\mu = 9.0$, $T = 273°K$, a point at which the outrider criteria were nearly, but not quite, fulfilled.

For $p_{HCl}(\mu,T)$ a similar procedure was followed, except that

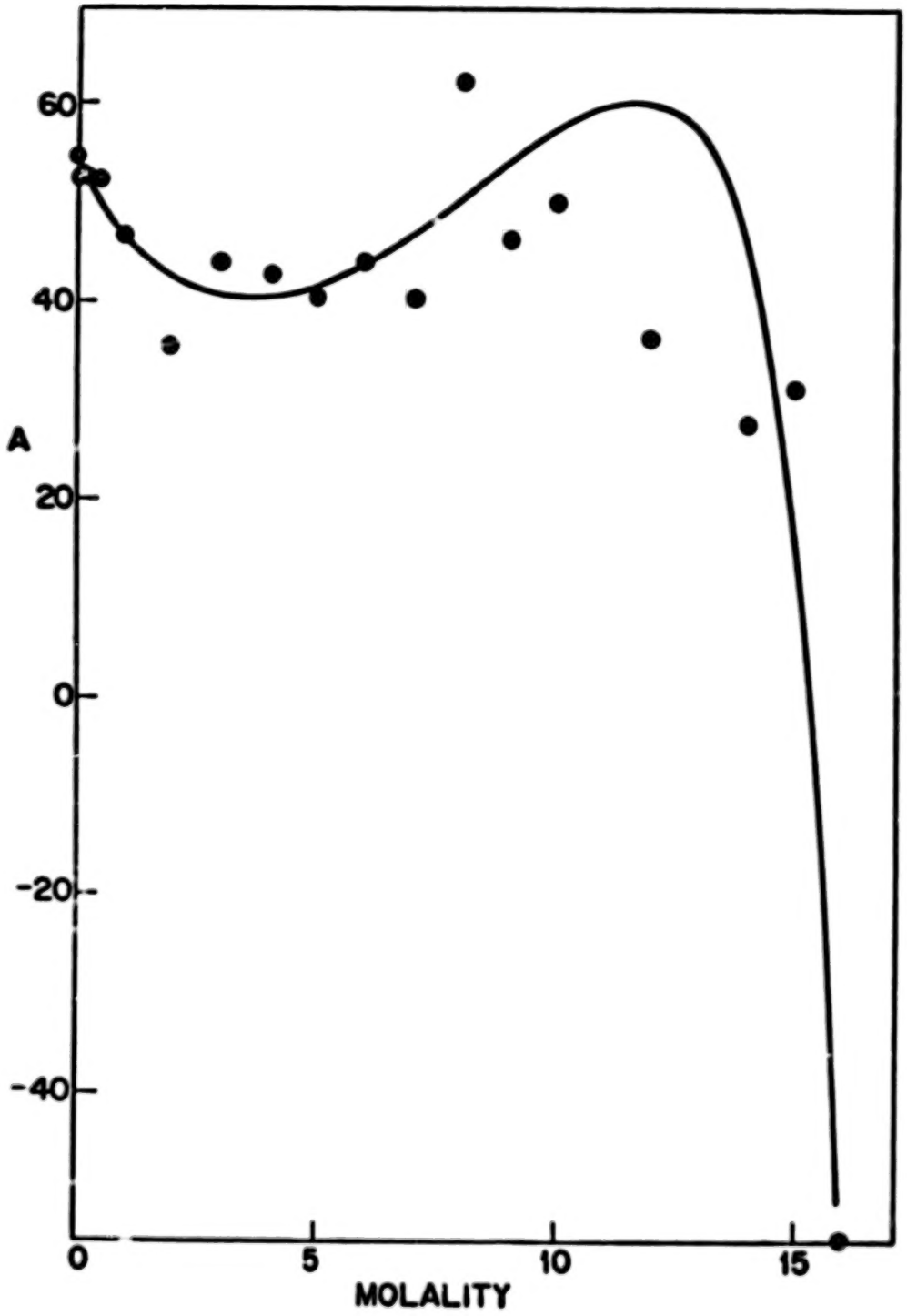

Fig. 4.1: Coefficienta A_0 vs μ and the Smoothed Curve $A_3(\mu)$.

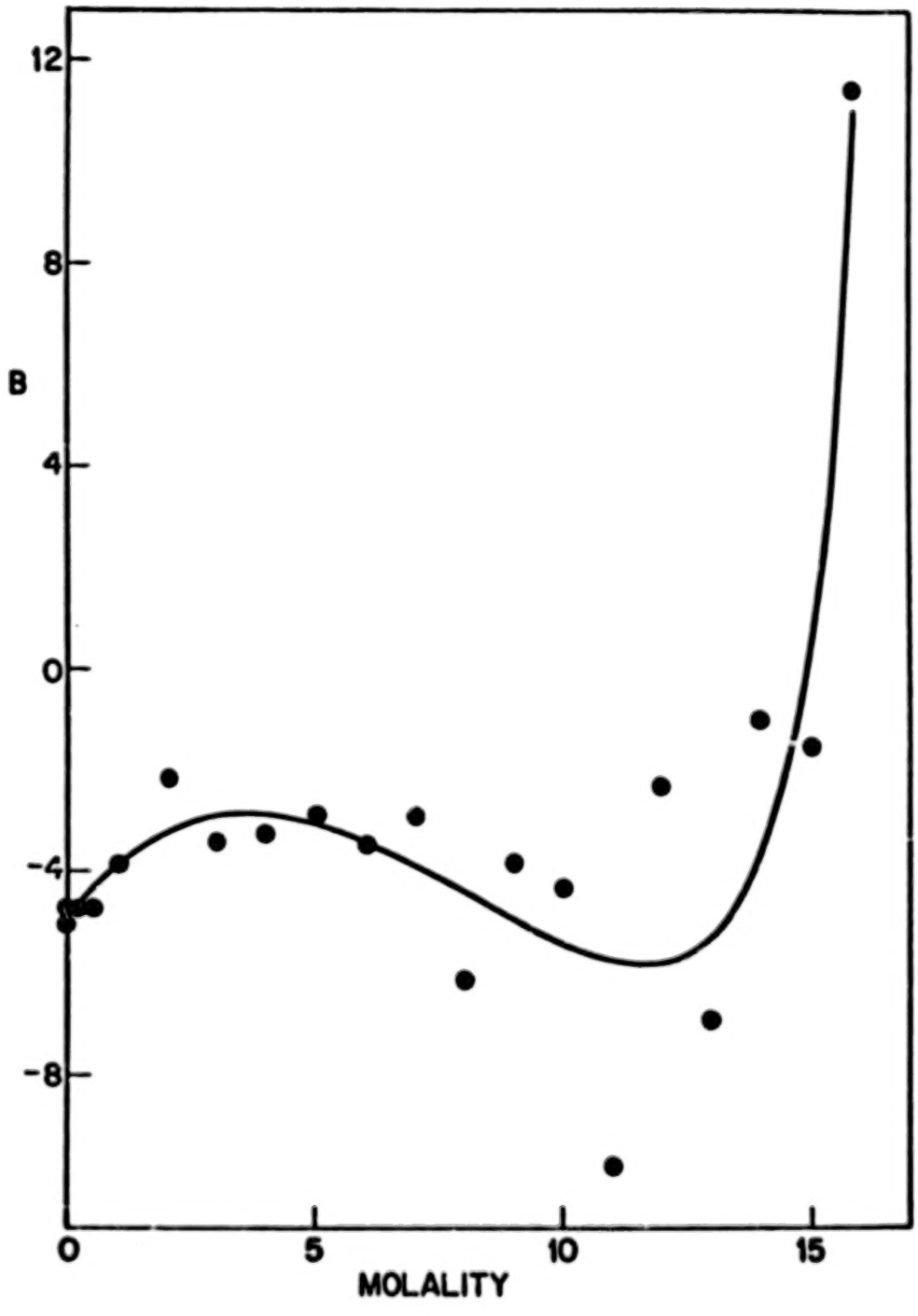

Fig. 4.2: Coefficients B_0 vs μ and the Smoothed Curve $B_2(\mu)$.

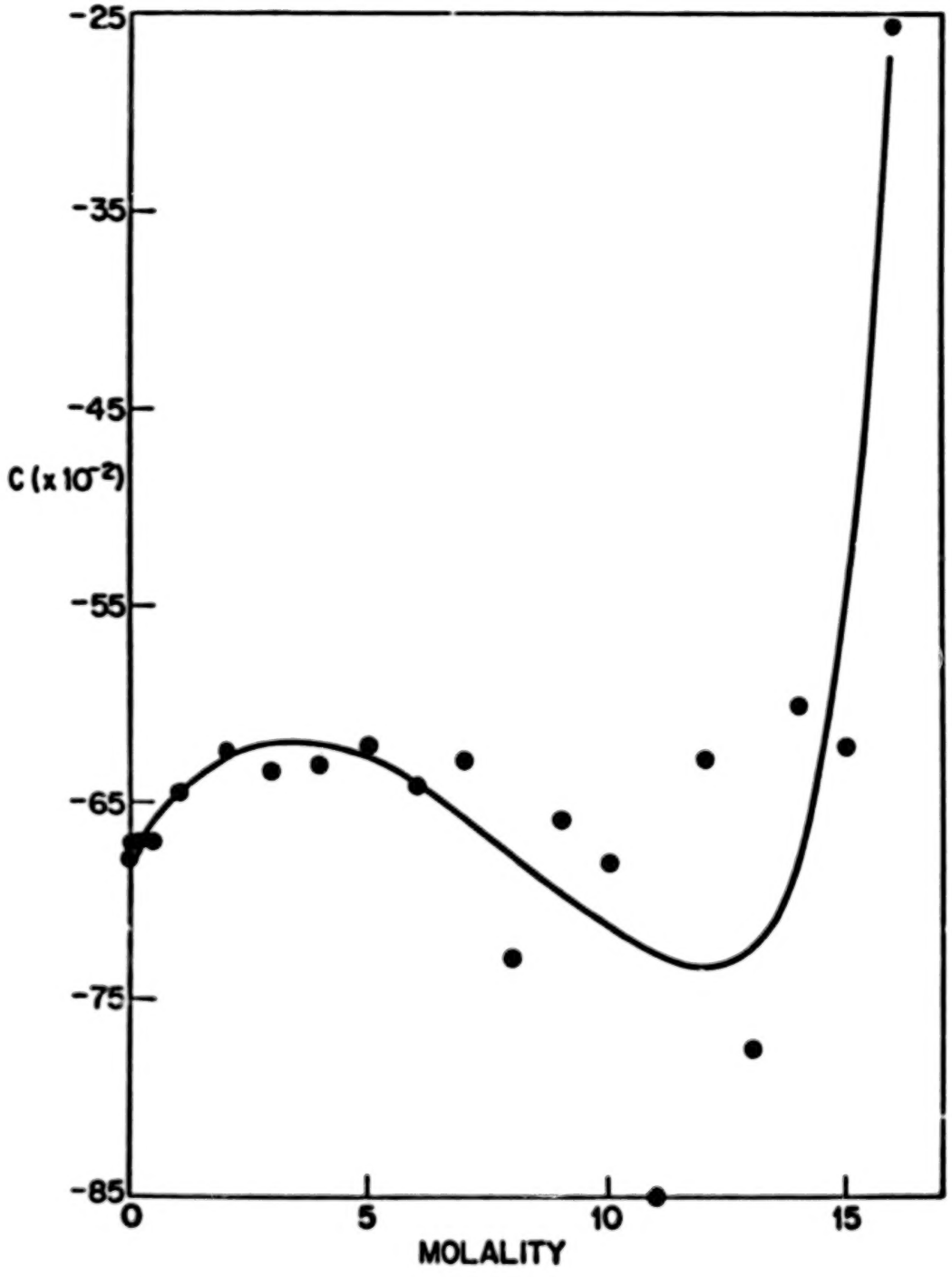

Fig. 4.3: Coefficients C_0 vs μ and the Smoothed Curve $C_1(\mu)$.

$$\ln p_{HCl} = A'(\mu) + B'(\mu)T^{-1} + C'(\mu)T^{-2} \qquad (7)$$

was used instead of (3). In turn, the coefficients are related somewhat differently to μ (Figures 4.4, 4.5, 4.6).

In this case $A'_1(\mu)$ was computed first by smoothing the data of Figure 44 obtaining

$$A'_1(\mu) = 30.542 - 1.3279\mu + 0.03242\mu^2 + 1.6501 \ln \mu$$

then computing $B'_1(\mu)$, $C'_1(\mu)$ and smoothing the former to get

$$B'_2(\mu) = -14694 + 987.61\mu - 24.308\mu^2 + 55.001 \ln \mu$$

and again recomputing to get $C'_2(\mu)$ and smoothing to get

$$C'_3(\mu) = 910.16 \times 10^3 - 158.00 \times 10^3 + 2045.9\mu^2 + 6331.4 \ln \mu + 23439\mu \ln \mu.$$

The final form for the equilibrium HCl vapor pressure is

$$\ln p_{HCl}(\mu,T) = A'_1(\mu) + B'_2(\mu)T^{-1} + C'_3(\mu)T^{-2} \qquad (8)$$

The overall average error given by this formulation as compared to the Fritz and Fuget (1956) values is about 1 per cent. The worst predictions are found at the low molalities and reach up to 4.6 percent error. This is not as good as it probably should be, and the study is continuing to determine whether a better choice of functional parameters can be made.

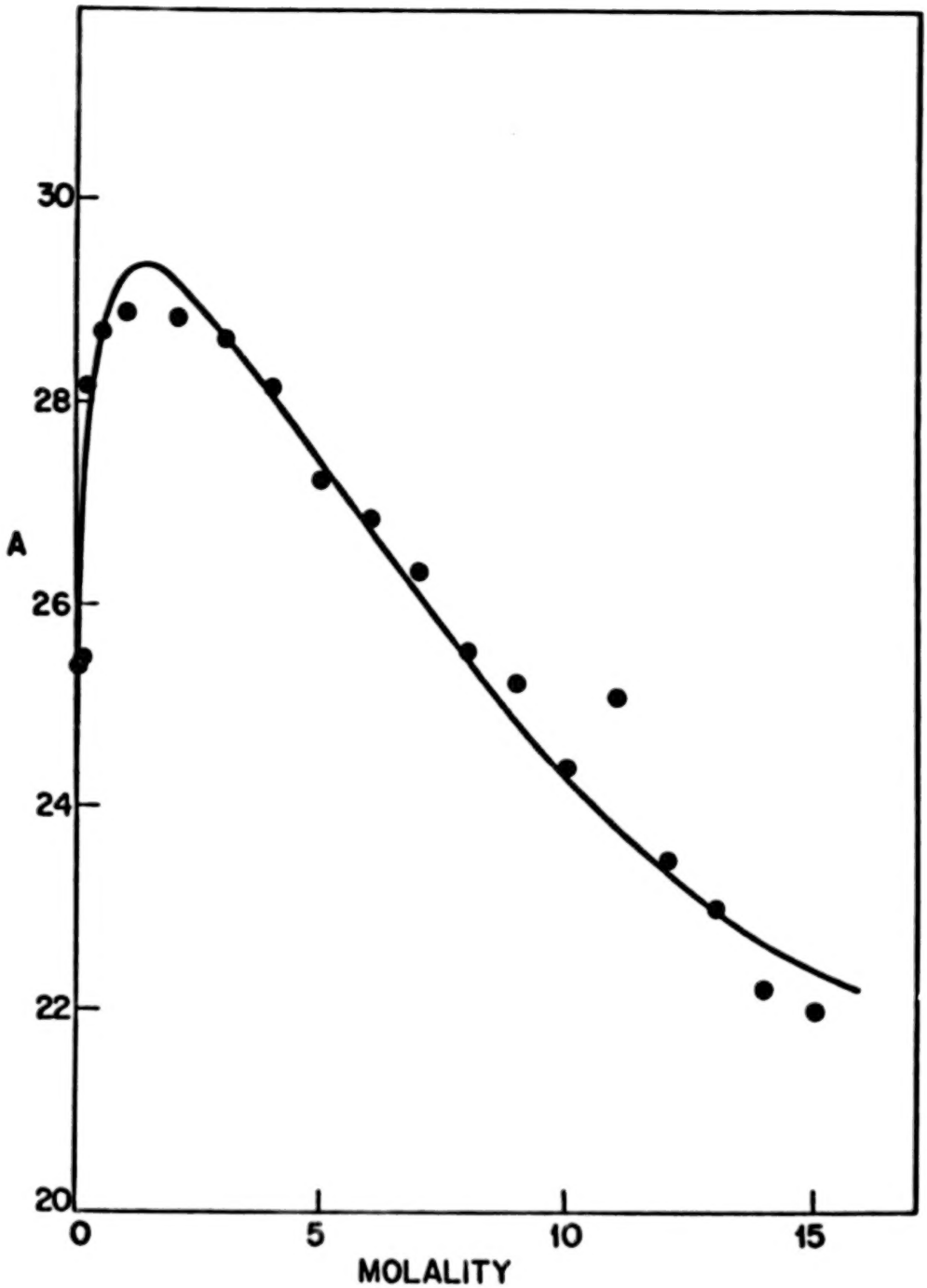

Fig. 4.4: Coefficients A' vs μ and the Smoothed Curve $A'_1(\mu)$.

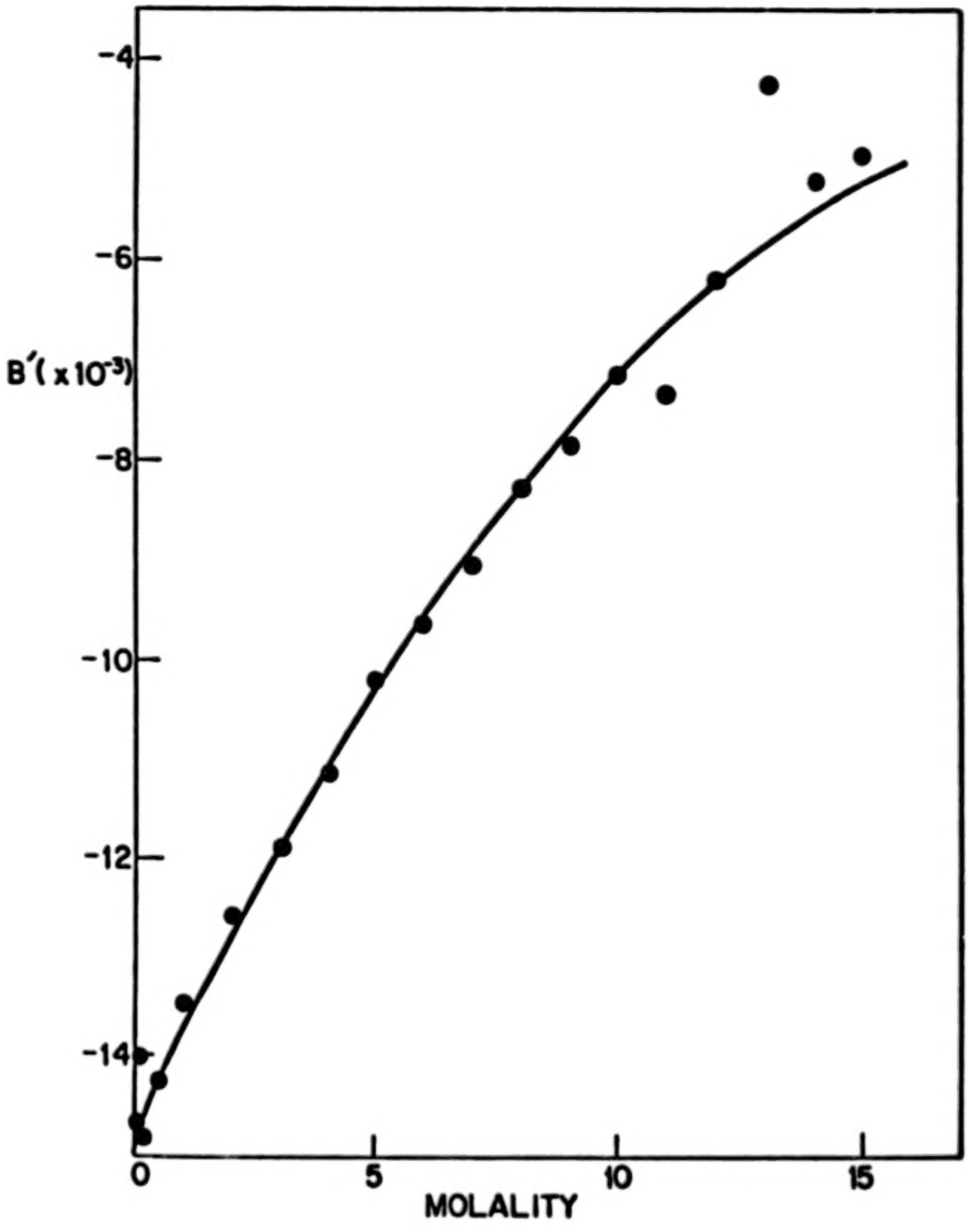

Fig. 4.5: Coefficients B' vs μ and the Smoothed Curve $B_2'(\mu)$.

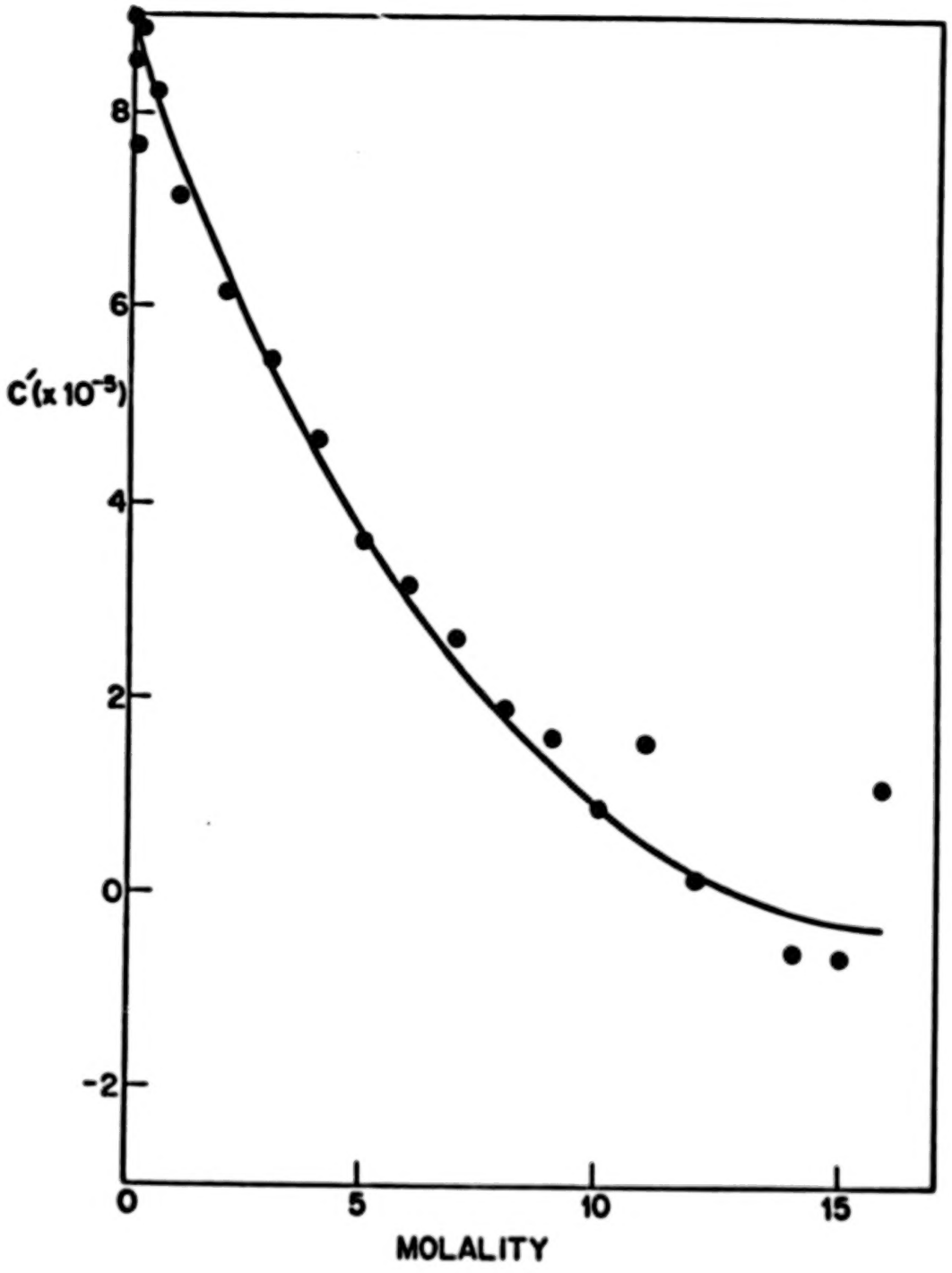

Fig. 4.6: Coefficients C' vs μ and the Smoothed Curve $C'_3(\mu)$.

REFERENCES

Fritz, J.J. and C.R. Fuget, 1956: Vapor Pressure of Aqueous Hydrogen Chloride Solutions, 0° to 50°C, Industrial and Engineering Chemistry, Chemical and Engineering Data Series, 1(1), 10-12.

1. Report No.	2. Government Accession No.	3. Recipient's Catalog No.
NASA CR-2928		

4. Title and Subtitle	5. Report Date
Rain Scavenging of Solid Rocket Exhaust Clouds	January 1978
	6. Performing Organization Code

7. Author(s)	8. Performing Organization Report No.
A. Nelson Dingle	014311-2-P
	10. Work Unit No.

9. Performing Organization Name and Address	11. Contract or Grant No.
Department of Atmospheric & Oceanic Science College of Engineering University of Michigan Ann Arbor, Michigan 48109	NSG 1243
	13. Type of Report and Period Covered
12. Sponsoring Agency Name and Address	Contractor Annual Report 10/75 - 12/76
National Aeronautics & Space Administration Washington, DC 20546	14. Sponsoring Agency Code

15. Supplementary Notes

Langley technical monitor: Gerald L. Pellett

Topical report.

16. Abstract The explicit model for cloud microphysics is developed for application to the problem of co-condensation/vaporization of HCl and H_2O in the presence of Al_2O_3 particulate nuclei. Validity of the explicit model relative to the implicit model, which has been customarily applied to atmospheric cloud studies, is demonstrated by parallel computations of H_2O condensation upon $(NH_4)_2\ SO_4$ nuclei.

A mesoscale predictive model designed to account for the impact of wet processes on atmospheric dynamics is also under development. It is found that the models of Pielke (1974) and of Pielke and Mahrer (1975) are relatively useful for dry (unsaturated) air dynamics, but that accounting for the impact of the wet processes requires extensive modification of these dry models. A more sophisticated treatment of boundary layer dynamics and the adaptation of the wet process parameterization scheme suggested by Kuo (1965) are proposed for the present model and are in process of formulation.

Input data specifying the equilibrium state of HCl and H_2O vapors in contact with aqueous HCl solutions are found to be limited, particularly in respect to temperature range (0 to 50°C). Extrapolation of the experimental data of Fritz and Fuget (1956) to atmospheric cloud temperatures by curve-fitting techniques, using the physical relationships indicated by thermodynamic theory, is formulated. The resulting formulae for smoothing, extrapolating, and interpolating the data are presented. Additional study of this sort is also underway for the adaptation of existing data on density, surface tension, and heats of solution and dilution.

17. Key Words (Suggested by Author(s))	18. Distribution Statement
Explicit model for cloud microphysics; Co-condensation of HCl and H_2O; Mesoscale wet process model; Input data formulation	Unclassified - Unlimited Subject Category 47

19. Security Classif. (of this report)	20. Security Classif. (of this page)	21. No. of Pages	22. Price*
Unclassified	Unclassified	62	$5.25

*For sale by the National Technical Information Service, Springfield, Virginia 22161

NASA-Langley, 1978

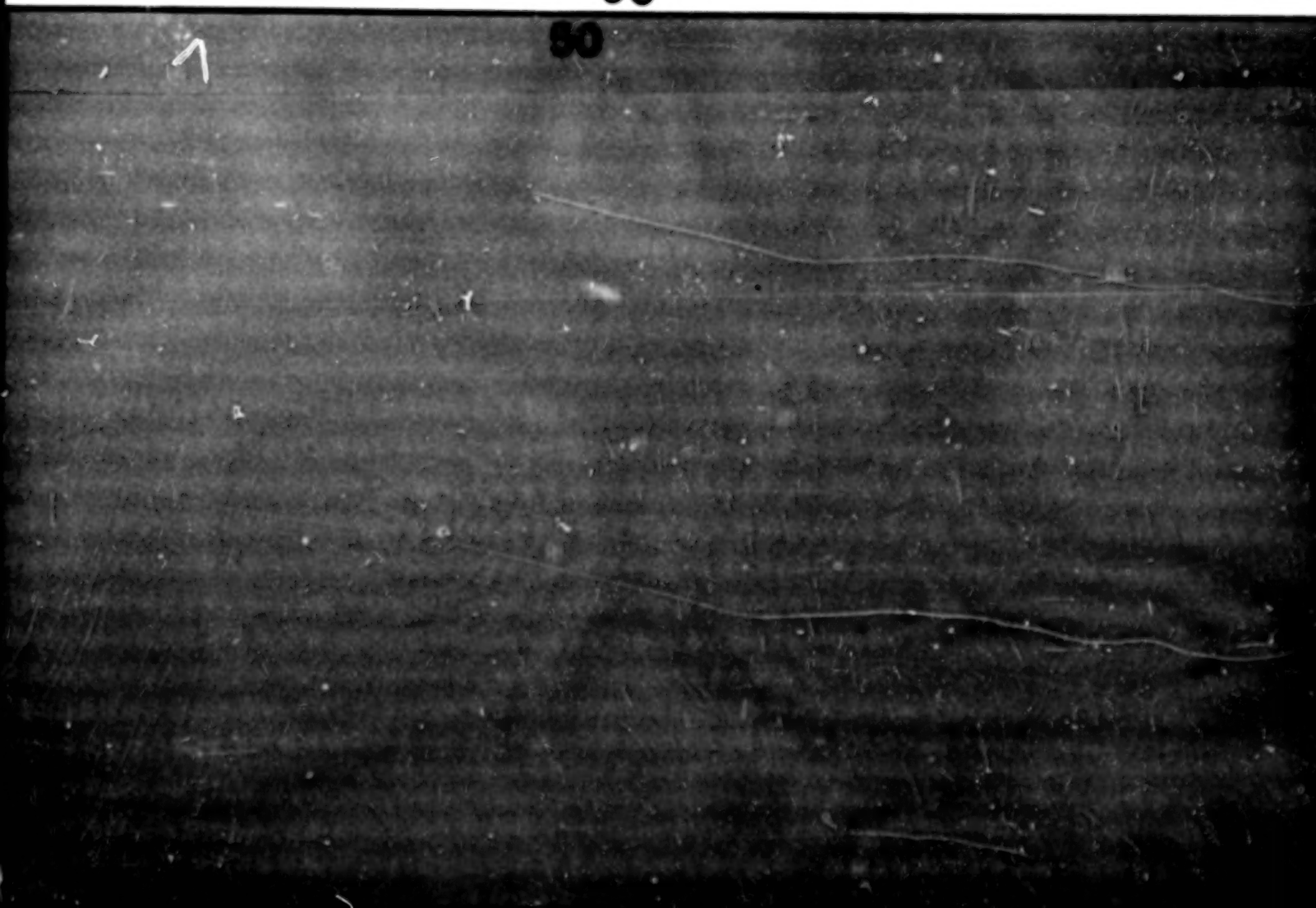
80

END

4.20.78